Flexibility of *Acanthamoeba* Myosin Rod Minifilaments

M. Jolanta Redowicz,[‡,⊥] John A. Hammer, III,[‡] Blair Bowers,[‡] Michal Zolkiewski,[§] Ann Ginsburg,[§] Edward D. Korn,[‡] and Donald C. Rau*[,∥]

Laboratory of Cell Biology and Laboratory of Biochemistry, National Heart, Lung, and Blood Institute, and Laboratory of Physical and Structural Biology, National Institute of Child Health and Human Development, National Institutes of Health, Bethesda, Maryland, 20892

Received November 10, 1998; Revised Manuscript Received February 9, 1999

ABSTRACT: Previous electric birefringence experiments have shown that the actin-activated Mg^{2+}-ATPase activity of *Acanthamoeba* myosin II correlates with the ability of minifilaments to cycle between flexible and stiff conformations. The cooperative transition between conformations was shown to depend on Mg^{2+} concentration, on ATP binding, and on the state of phosphorylation of three serines in the C-terminal end of the heavy chains. Since the junction between the heavy meromyosin (HMM) and light meromyosin (LMM) regions is expected to disrupt the α-helical coiled-coil structure of the rod, this region was anticipated to be the flexible site. We have now cloned and expressed the wild-type rod (residues 849−1509 of the full-length heavy chain) and rods mutated within the junction in order to test this. The sedimentation and electric birefringence properties of minifilaments formed by rods and by native myosin II are strikingly similar. In particular, the Mg^{2+}-dependent flexible-to-stiff transitions of native myosin II and wild-type rod minifilaments are virtually superimposable. Mutations within the junction between the HMM and LMM regions of the rod modulate the ability of Mg^{2+} to stabilize the stiff conformation. Less Mg^{2+} is required to induce minifilament stiffening if proline-1244 is replaced with alanine. Deleting the entire junction region (25 amino acids) results in a even greater decrease in the Mg^{2+} concentration necessary for the transition. The HMM−LMM junction does indeed seem to act as a Mg^{2+}-dependent flexible hinge.

Myosin II from *Acanthamoeba castellanii* provides a striking example of the functional interaction between the head and tail domains of a conventional myosin. Structurally, this myosin resembles other class-II myosins; i.e., it is composed of a pair of heavy chains and two pairs of light chains (*1*, *2*). Each 171-kDa heavy chain folds into an N-terminal ∼90-kDa globular head that has the actin-binding (*3*) and ATPase (*4*) sites that are responsible for mechanochemical activity of myosin. The ∼81-kDa C-terminal tails of the two heavy chains form an α-helical coiled-coil, 90-nm-long rod (∼40% shorter than the rod of skeletal muscle myosin) that mediates formation of 210−230-nm-long antiparallel minifilaments (*2*−*5*) comprised of eight myosin II monomers (*6*, *7*).

The C-terminal, nonhelical 27 amino acids of each heavy chain contains 3 serine residues that can be phosphorylated in vivo (*8*, *9*) and by a myosin II heavy chain kinase in vitro (*10*). Phosphorylation of these sites at the C-terminus of the rods inactivates the actin-activated Mg^{2+}-ATPase (*10*, *11*) and the in vitro motility activities (*12*) associated with the N-terminal heads of myosin II minifilaments. However, in contrast to the regulation of certain other class-II myosins by heavy or light chain phosphorylation (reviewed in refs *13*, *14*), there is no evidence for direct head−tail interactions in *Acanthamoeba* myosin II or that formation of minifilaments is inhibited by phosphorylation. Instead, the evidence (*15*−*17*) suggests that regulation is a consequence of the cooperative interaction of myosin monomers within the minifilament rather than a property of individual myosin molecules. Proteolytic studies also show that the conformation of myosin II heads is coupled to the state of phosphorylation of the tail and, conversely, that ATP bound to myosin II heads affects the conformation of the C-terminal tail of phosphorylated minifilaments (*18*). The thermal unfolding of monomeric *Acanthamoeba* myosin II, which differs from the unfolding of rabbit skeletal muscle myosin, also indicates high cooperativity between head and tail domains (*19*). All of these properties suggest functional communication between the N-terminal heads and C-terminal tails of *Acanthamoeba* myosin II.

Electron microscopy and the amino acid sequence of *Acanthamoeba* myosin II indicate the presence of a potential hinge region, about 30 kDa from the C-terminus (*5*). This 22 amino acid domain, which defines the junction between the N-terminal heavy meromyosin (HMM)[1] and C-terminal light meromyosin (LMM) domains, contains an α-helix-

* Address correspondence to this author at the National Institutes of Health, Building 9, Room 1E122, Bethesda, MD 20892-0924. Fax: (301) 402-9462. E-mail: donrau@helix.nih.gov.

[‡] Laboratory of Cell Biology, National Heart, Lung, and Blood Institute.

[§] Laboratory of Biochemistry, National Heart, Lung, and Blood Institute.

[∥] Laboratory of Physical and Structural Biology, National Institute of Child Health and Human Development.

[⊥] Present address: Department of Muscle Biochemistry, Nencki Institute of Experimental Biology, Warsaw, Poland.

[1] Abbreviations: A_{slow}, signal amplitude of the slow, negative birefringence component; A_{fast}, signal amplitude of the fast, positive birefringence component; HMM, heavy meromyosin; LMM, light meromyosin; S1, myosin subfragment-1; S2, myosin subfragment-2; τ_{slow}, relaxation time of the slow, negative birefringence component; $\langle\tau_{fast}\rangle$, average relaxation time of the fast, positive birefringence component.

10.1021/bi982679d
Published on Web 05/11/1999

breaking proline residue (Pro-1244) and additional perturbations of the heptad repeat that is characteristic of α-helical coiled-coils (reviewed in ref *20*). Electron microscopy of myosin II minifilaments (*6*, *7*) and electric birefringence experiments on parallel dimers (*21*) indicate that the hinge region of one monomer could be in close proximity to the phosphorylatable tailpiece of another monomer in the minifilament, suggesting that phosphorylation-induced changes in hinge conformation could be the mechanism for communication between the head and tail regions (*22*).

This supposition is supported by recent electric birefringence studies showing that the flexibility of *Acanthamoeba* myosin II minifilaments is affected by both phosphorylation of the tail (*23*) and nucleotide bound to the head (*24*). Specifically, enzymatically active, dephosphorylated minifilaments are 50 times more rigid than inactive, phosphorylated minifilaments at 4−5 mM Mg^{2+} (conditions that are nearly optimal for actin-activated Mg^{2+}-ATPase activity), and bound ATP substantially increases the flexibility of dephosphorylated minifilaments but has no effect on the flexibility of phosphorylated minifilaments. These observations suggest that actin-activated Mg^{2+}-ATPase activity may not only correlate with, but also depend on the ability of myosin II minifilaments to oscillate between stiff and flexible conformations during the ATP hydrolysis cycle. Active, dephosphorylated minifilaments are able to cycle between flexible and stiff conformations while inactive, phosphorylated filaments are restricted to the flexible conformation (*24*).

To evaluate further the importance of the hinge region in the structure and flexibility of myosin II minifilaments, we have cloned wild-type myosin II rod and two hinge-mutant rods: a point mutant, with alanine substituted for proline-1244; and a deletion mutant, with the entire hinge region (residues 1230−1254) removed. We reported previously on the thermal unfolding and analytical ultracentrifugation of monomers of these rods (*25*). We now report evidence from electron microscopy, analytical ultracentrifugation, and, principally, electric birefringence that the magnitude and Mg^{2+} dependence of the flexibility of rod minifilaments parallel the predicted probability that the hinge region between the HMM and LMM domains will form a stable, α-helical coiled-coil.

EXPERIMENTAL PROCEDURES

Proteins. The purification of native myosin II from *Acanthamoeba castellanii* (*26*, *27*) and the expression and purification of wild-type, point mutant, and deletion mutant rods (*25*) have been described. Proteins were stored at 4 °C in buffer containing 20 mM imidazole, pH 7.5, 0.3 M KCl, and "Complete" tablets (Boehringer Mannheim) to inhibit proteolysis. As determined by SDS−PAGE, the preparations were ∼95% pure. The apparent molecular masses of the wild-type and point mutant peptide chains were 82 kDa (theoretical masses: 74 kDa), and the apparent mass of the deletion mutant was 72 kDa (theoretical mass: 71.4 kDa). Protein concentrations (which could not be accurately determined by A_{280} because there are only two tyrosine residues per peptide chain) were determined by circular dichroism using a Jasco, Inc., Model J-710 spectrometer. Because of their very high α-helical content, a 1.0 mg/mL solution of monomeric myosin II rod gave a signal of −82.60 mdeg at 222 nm in an 0.2-mm path-length cylindrical cell at 25 °C (*25*).

Electron Microscopy. Rod monomers were dialyzed overnight against 0.8 M ammonium acetate, pH 7.5; the final protein concentrations were about 0.06 mg/mL. The samples were mixed with 2 volumes of glycerol and sprayed against freshly cleaved mica, as described by Tyler and Branton (*28*). The specimens were rotary-shadowed with platinum at room temperature at an angle of 7° in a Balzers 301 freeze−fracture apparatus fitted with electron guns.

Analytical Ultracentrifugation. Myosin rod monomers (0.12−0.14 mg/mL) were dialyzed against 5 mM $MgCl_2$, 20 mM KCl, and 20 mM potassium phosphate buffer, pH 7.5, to form minifilaments. The Optima Model XL-A (Beckman, Inc.) analytical ultracentrifuge equipped with a four-place An-Ti rotor was used for sedimentation velocity experiments at 20.0 °C. The density (ρ) and relative viscosity (η/η_0) of the dialysate buffer were determined to be 1.00355 g/mL at 20.00 ± 0.01 °C with a Paar DMA 58 densitometer and 1.010 (*29*), respectively. The partial specific volume of wild-type and mutant rods calculated from the amino acid sequence (*5*) was 0.73 mL/g (*30*). Protein samples (0.34 mL) were loaded into the right side of a 4° Kel-F-coated double-sector centerpiece, and the dialysate buffer (0.35 mL) was placed in each left sector of a 12-mm cell equipped with plane UV quartz windows. After equilibration at 20.0 °C, radial calibrations, and wavelength scans (11 averages at 1-nm resolution) at 3000 rpm, the rotor was accelerated to 20 000 or 25 000 rpm, and radial scans of the cells were performed at 230 nm (in the continuous mode with 0.003-cm steps and triple averaging). Observed sedimentation coefficients (s_{obs}) were calculated as before (*25*) and corrected to values in water at 20.0 °C ($s_{20,w} = 1.02475 s_{obs}$). In all cases, the 230-nm absorbances of plateau regions agreed with values initially determined spectrophotometrically. Sedimentation and diffusion coefficients were calculated from 4−6 successive, late radial scans by the time-derivative method of Stafford (31−33) using software supplied by Beckman, Inc. Gaussian fits to $g(s^*)$ vs s^* patterns were performed on unsmoothed data. Molecular weights (M_r) of minifilaments were calculated from the Svedberg equation: $M_r = RTs/[D(1 - \bar{v}\rho)]$. Because sedimentation rates were low, the results obtained at 25 000 rpm were found to be more reliable than those obtained at 20 000 rpm, and therefore only the former were used in statistical averaging.

Electric Birefringence. Stock solutions of rods (final concentrations: 0.2−0.4 mg/mL) were extensively dialyzed against 2.5 mM imidazole (pH 7.4) and 20 mM KCl. Rods were polymerized by diluting the protein to about 15−30 μg/mL, adjusting to 2 mM KCl and 2 mM imidazole (pH 7.4), and then adding $MgCl_2$ in aliquots with mixing to obtain the desired Mg^{2+} concentrations. A description of the electric birefringence technique and the instrumentation used has been given elsewhere (*21*, *23*, *24*). Very briefly, an externally applied electric field is used to orient minifilaments in solution. This orientation causes a small rotation of the polarization plane of laser light (a birefringence) as it passes through the sample. This angle, δ (typically ∼0.01° in the present experiments), can be measured by monitoring changes in the optical signal intensity as the light is passed through a subsequent $\lambda/4$ wave plate and polarizer set nearly perpendicular to the initial polarization angle. As was also

noted previously for native myosin II (*23*, *24*), rod minifilaments can begin to aggregate under certain experimental conditions. High protein concentrations, extended signal averaging, long field pulses, or high field strengths all led first to a slowly decaying tail in the birefringence signal and eventually to turbid solutions. To avoid this problem, standard conditions for the rod birefringence experiments reported here were a protein concentration of about 15−30 μg/mL, a field strength $E \sim 1.4$ kV/cm, and a voltage pulse length of 65 μs. Optical signals from a single sample were averaged over 32 pulses. No aggregation was observed with these conditions. Signal amplitudes were measured as a function of field strength, E, up to about 2 kV/cm to verify that the rotation angle δ scales with E^2, showing that orientation energies were small compared with the thermal energy kT. Signal amplitudes were also observed to vary linearly with protein concentration up to the highest concentrations used, about 30 μg/mL.

Slow component relaxation times were extracted from the decay of the optical signal after the applied electric field is removed both directly from the slope of the semilog plot of signal intensity vs time at long times (>50 μs after the end of the pulse) and from fits of the entire decay curve to a double exponential function. The birefringence base line was taken from the data 800−1200 μs after the end of the pulse. The relaxation times of the fast, positive birefringence component were also determined from the double exponential function fits to experimental curves both with a 65-μs pulse length and $E \sim 1.4$ kV/cm, and with shorter pulse lengths ($\sim$10 μs), higher field strengths, $\sim$3 kV/cm, and averaging a larger number of signals (typically $\sim$128). Under the latter condition, the positive birefringence component dominates the observed signal. The slowly decaying component can be well fit by a single exponential. We are less certain that the positive birefringence component has only a single relaxation time. The fast decay times are reported as average values, $\langle\tau_{fast}\rangle$, to emphasize this point.

Rotational diffusion coefficients for the spinning and tumbling motions of the whole minifilament were calculated using the formalism of Garcia de la Torre and Bloomfield (*34*). Rods were modeled as an assembly of 1-nm radius beads. The overall length of a monomer was taken as 94 nm, assuming 0.148 nm/amino acid in an α-helical coiled-coil (*35*, *36*). Minifilaments were assumed to be octamers (*6*, *7*). The beads modeling the LMM domain were packed as a square lattice for the minifilament backbone (along the x-axis). The four subfragment-2 (S2) equivalents of the rods on each end were staggered by 15 nm and allowed to bend in the $x-y$ plane. The entire structure was centrosymmetric. Iterative calculation of frictional coefficients was continued until the difference between successive calculations was less than 0.1%. There are essentially two principal frictional coefficients: F_ϕ, for the spinning rotation of the long axis; and F_θ, for the tumbling about the long axis. The observed fast and slow component relaxation times are given by $1/\tau_{fast} = 2kT(1/F_\theta + 2/F_\phi)$ and $1/\tau_{slow} = 6kT/F_\theta$, respectively (*37*).

RESULTS

Prediction of Coiled-Coil Formation by Myosin II Rods. N-terminal microsequencing showed that all three rod sequences began with isoleucine-849 (for convenience, the sequence numbering of native *Acanthamoeba* myosin II will be maintained for the rods). Proline-847 is generally considered to define the head−tail boundary. Myosin II rods are well-known to form an α-helical coiled-coil dimer characterized by an amino acid sequence with heptad repeats *abcdefg*, with residues *a* and *d* generally hydrophobic (*20*). The assignment of the heptad phasing of the wild-type *Acanthamoeba* myosin II rod sequence by the program Paircoil (*38*) is shown in Figure 1. The probability of coiled-coil formation at any position along the sequence of the wild type, point mutant, and deletion mutant rods as predicted by Paircoil is given in Figure 2. Very similar results were obtained when the sequence was analyzed by the program Coils (*39*). Except for three regions, both programs predict a 100% probability of a stable α-helical coiled-coil structure for the wild-type rod (Figure 2a). Both programs predict that the coiled-coil structure is completely disrupted at Pro-1244. Paircoil predicts the region around this proline between Arg-1227 and Gly-1247 has a reduced probability of about 85% to form a coiled-coil, thus forming a potential hinge region between the HMM and LMM domains. Coils predicts about

```
                defgabcdefgabcdefgabcdefgabc
848                      LISQRNFQKEIDD  860
861  LKKQVKDLEKELAALKDANAKLDKEKQL  888
889  AEEDADKLEKDLAALKLKILDLEGEKAD  916
917  LEEDNALLQKKVAGLEEELQEETSASND  944
945  ILEQKRKLEAEKGELKASLEEEERNRKA  972
973  LQEAKTKVESERNELQDKYEDEAAAHDS 1000
1001 LKKKEEDLSRELRETKDALADAENISET 1038
1039 LRSKLKNTERGADDVRNELDDVTATKLQ 1056
1057 LEKTKKSLEEELAQTRAQLEEEKSGKEA 1084
1085 ASSKAKQLGQQLEDARSEVDSLKSKLSA 1112
1113 AEKSLKTAKDQNRDLDEQLEDERTVRAN 1140
1141 VDKQKKALEAKLTELEDQVTALDGQKNA 1178
1179 AAAQAKTLKTQVDETKRRLEEAEASAAR 1196
1197 LEKERKNALDEVAQLTADLDAERDSGAQ 1224
                    HINGE •
1225 QRRKLNT---RISELQSELENAPKTGGA 1249
1250 SSEEVKRLEGELERLEEELLTAQEARAA 1277
1278 AEKNLDKANLELEELRQEADDAARDNDK 1305
1306 LVKDNRKLKADLDEARIQLEEEQDAKSH 1333
1334 ADSSSRRLLAEIEELKKRVAKETSDKQK 1361
1362 AQDQKANYQRENESLKADRDSIERRNRD 1389
1390 AERQVRDLRAQLDDALSRLDSEKRAKEK 1417
                       ••••••••
1418 SVEANRELKKVVLDRERQSLESLSKF-- 1445
1446 ----NSALESDKQILEDEIGDLHEKNKQ 1473
                     TAILPIECE
                    ••••••••••••
1474 LQAKIAQLQDEIDGTPSSRGGSTRGASA 1501
     ••••••••••••
1502 RGASVRAGSARAEE              1509
```

FIGURE 1: Amino acid sequence of the *Acanthamoeba* myosin II rod with heptad repeat and residue assignment according to Paircoil. Residues with a bullet over them were not assigned by Paircoil. The sequence begins at L848 (using the sequence numbering for native *Acanthamoeba* myosin II) which follows P847 that defines the separation between the S1 and S2 segments of the HMM domain. The hinge region at the junction between the HMM and LMM domains (R1227−T1246), a second region with low probability of forming a coiled-coil (L1430−S1445), and the completely nonhelical C-terminal tailpiece (P1483−E1509) are italicized. P1244, in the hinge region, and P1483, at the beginning of the tailpiece, are in boldface type. The three serines in the tailpiece whose phosphorylation regulates actin-activated ATPase activity are underlined. Paircoil was used interactively (http://nightingale.lcs.mit.edu/cgi-bin/score).

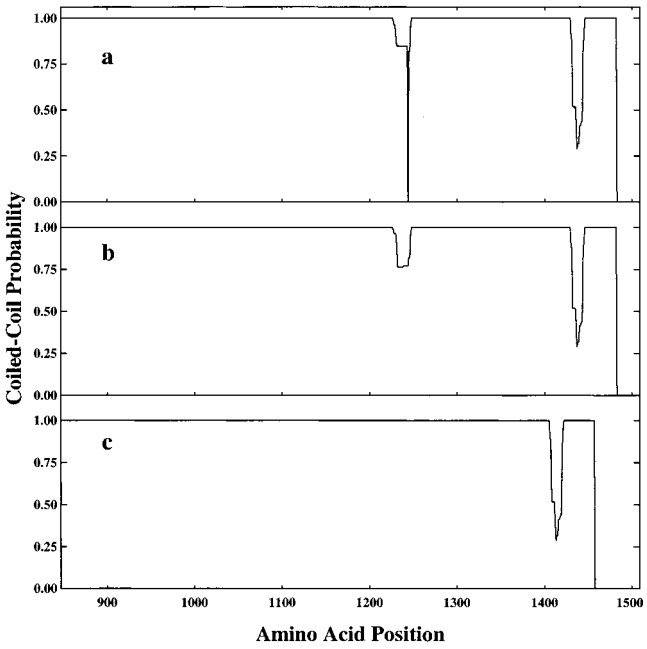

FIGURE 2: Graphical representation of the probability that an amino acid residue is in an α-helical coiled-coil conformation for the wild-type (a), point mutant (b), and deletion mutant (c) *Acanthamoeba* myosin II rods according to Paircoil. Similar results were obtained with the Coils program MTK (http://www.isrc.isb-sib.ch/coils/COILS_doc.html) with the residues at positions *a* and *d* (Figure 1) given a weight of 2.5.

90% probability for forming a coiled-coil within this region. A second region between Leu-1430 and Ser-1445 is predicted to have only a 30% (Paircoil) or 75% (Coils) probability of forming a coiled-coil. Consistent with this prediction, Phe-1443 is susceptible to chymotrypsin cleavage (*10*). Last, the final 27 amino acids (Pro-1483 to Glu-1509), that include the 3 phosphorylatable serines, are predicted by both Paircoil and Coils to form a completely nonhelical tailpiece. Both Paircoil and Coils predict that substitution of Ala for Pro-1244 eliminates the complete disruption of the coiled-coil at that position (Figure 2b), but only reduces slightly the probability of coiled-coil formation for the remainder of the hinge region. Deletion of the 25 amino acids Asn-1230 to Val-1254 (3 complete heptads plus 4 additional amino acids) reestablishes the heptad repeat and leads to a predicted 100% probability of stable coiled-coil throughout the HMM−LMM junction (Figure 2c).

Size, Shape, and Homogeneity of Wild-Type and Mutant Rod Monomers and Minifilaments. As verified by electron microscopy (Figure 3 and Table 1), the wild-type and mutant rods were monomeric at high ionic strength with an average contour length of ~90 nm. Approximately 40% of wild-type rod monomers (compared to about 50% of native myosin II monomers), but only about 8% of the point and deletion mutant rod monomers, had a sharp kink at the position corresponding to the hinge region. The point and deletion mutant monomers were indistinguishable by electron microscopy. These observations are consistent with previous sedimentation velocity studies (*25*) that gave estimated lengths of 82 nm for wild-type rod monomers and 90 nm for both mutant rod monomers (as expected if the wild-type rod is more bent or flexible than the mutant rods). The absence of a sharp bend for the point and deletion mutant rod monomers indicates that Pro-1244 is the major contributor to the kink that separates the HMM and LMM domains. It is not clear if the kink is due to a static structure or a dynamic bending. No kink or bend was observed in any of the monomer preparations at the position corresponding to residues 1430−1445.

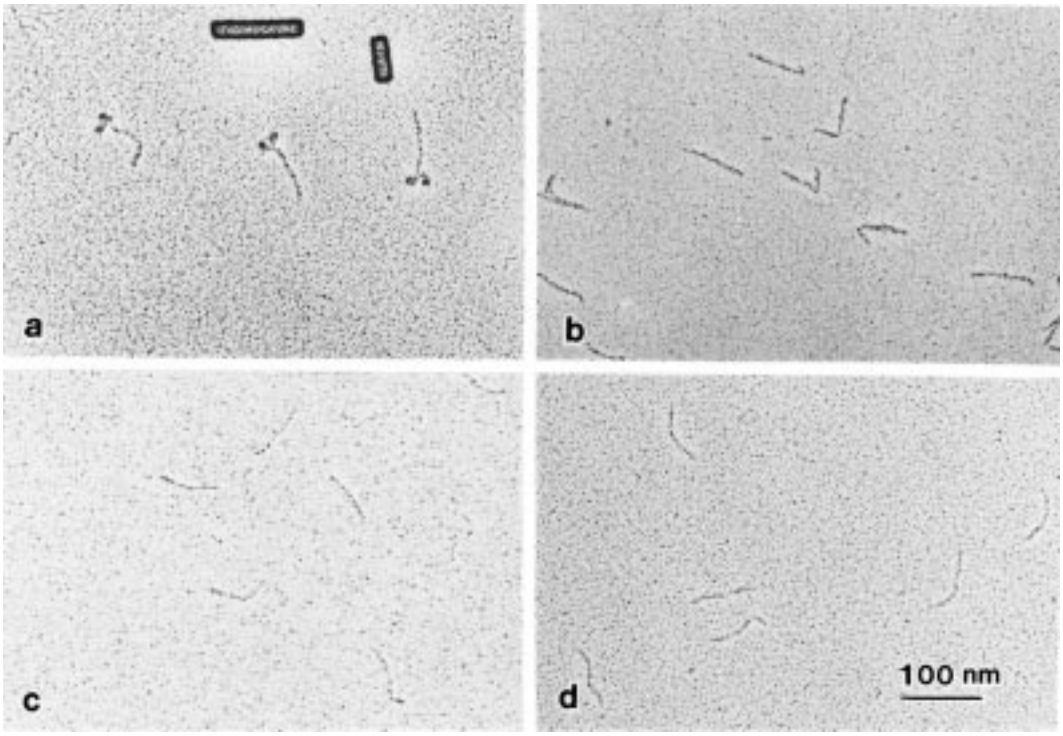

FIGURE 3: Rotary shadow electron microscopy of monomers of native *Acanthamoeba* myosin II (a) and wild-type (b), point mutant (c), and deletion mutant (d) rods. The rectangular images in (a) are tobacco mosaic viruses added to the sample to facilitate localization of the myosin monomers. See Experimental Procedures and Results for details.

Table 1: Statistical Analysis of Shadowed Images of Monomeric Rods[a]

monomer	straight or curved (%)	kinked (%)	no. scored
wild-type rod	58	42	401
point mutant	92	8	368
deletion mutant	92	8	198
native myosin II	50	50	193

[a] Shadowed rod monomers were examined at a magnification of 64400×.

Table 2: Sedimentation Properties of *Acanthamoeba* Myosin II Wild-Type and Mutant Rod Filaments[a]

rod	$s_{20,w}$ (S)	$M_r \times 10^{-6}$	M_r/M_{rod}	f/f_0
wild type	10.9	1.23	8 ± 1.0	3.7
point	10.6	1.22	8 ± 0.2	3.8
deletion	11.3	1.19	8 ± 0.3	3.5

[a] Myosin II minifilaments (0.12−0.14 mg/mL in 20 mM K-PO_4, 20 mM KCl, and 5 mM $MgCl_2$, pH 7.5) were centrifuged at 25 000 rpm and 20.0 °C. Sedimentation coefficients ($s_{20,w}$), in Svedberg units (S), were corrected for the density and viscosity of the buffer; estimated errors are ≤±0.06 S for *s* values. Molecular weight (M_r) values were calculated from the sedimentation and diffusion coefficients obtained from the maximum and half-width, respectively, of the Gaussian fit to the distribution function of apparent sedimentation coefficients using the time-derivative analysis of Stafford (*32*, *33*); see Experimental Procedures for further details. The number of coiled-coil rods in each minifilament was calculated from the observed M_r and rod molecular weights calculated from the amino acid sequences: 149K for the wild-type and point mutant rods and 144K for the deletion mutant (*5*). Frictional ratios (f/f_0) were calculated from the frictional coefficient $f = [M(1 - \bar{v}\rho)]/N_s$ and f_0 [the frictional coefficient of a sphere having a volume equal to that of an ellipsoid; $f_0 = 6\pi\eta(3M\bar{v}/4\pi N)^{1/3}$ (*40*)], assuming octameric structures and unchanged partial specific volumes for rod minifilaments.

The sedimentation properties of the rod minifilaments are summarized in Table 2. Single, symmetrical sedimenting boundaries (representing loading concentrations in plateau regions) were observed for wild-type and both mutant rod minifilaments (data not shown). In all cases, time derivatives of concentration profiles at late times yielded $g(s^*)$ vs s^* curve that were fit well by single Gaussians (data not shown), indicating that all three minifilament preparations were essentially homogeneous.

The molecular weights calculated from the sedimentation data indicate that the minifilaments of wild-type and mutant rods contain ∼8 coiled-coil rod monomers/filament (Table 2), consistent with previous measurements showing that native myosin II forms antiparallel, octameric minifilaments (*6*, *7*). The frictional ratios of the minifilaments of the wild-type, point, and deletion mutant rods calculated from the sedimentation data (Table 2) correspond to axial ratios for prolate ellipsoids of about 83, 88, and 74, respectively (*40*). These values are somewhat larger than the value of 67 for the rod domain of native myosin II minifilaments estimated by us from published electron micrographs (*6*, *7*, *41*), suggesting the importance of volume and packing effects that were not considered in the calculations. We were unable to measure reliable axial ratios from the rotary-shadowed electron microscopic images of the three rod preparations because the minifilaments were distorted by the high-pressure spraying required for sample preparation and the mutant rod minifilaments tended to aggregate.

Electric Birefringence. In 2 mM Mg^{2+}, the electric birefringence signals from wild-type and point mutant rod minifilaments and minifilaments of native, dephosphorylated myosin II were qualitatively similar (Figure 4a, b, and c, respectively). Both the buildup of the optical signal as the electric field was applied and its decay after the field was removed (indicated by the arrow) show that the overall signal is composed of a small amplitude, fast component with positive birefringence and a much slower, but much larger amplitude, negative birefringence component. The relative amplitudes of the fast and slow components were similar for native myosin and wild-type rod minifilaments (Figure 4a,b), but the relative amplitude of the fast, positive birefringence component was much smaller for the point mutant rod minifilaments (Figure 4c). The deletion mutant rod minifilaments showed virtually no signal at 2 mM Mg^{2+}. The birefringence signal at 1 mM Mg^{2+}, however, is shown in Figure 4d. The qualitative appearance of this signal is quite similar to that for the wild-type rod minifilaments

Since a symmetric bipolar filament has no inherent dipole, we argued previously (*23*, *24*) that a dipole moment is induced by a distortion of the minifilament structure, as, for example, by flexing of the HMM portions of the monomers within the filament in the direction of the applied electric field. This can explain the large negative birefringence component of the signal that indicates a very unusual perpendicular orientation of the long filament axis with respect to the applied electric field (*37*). The positive birefringence signal is due to a projection of the optical axis onto this perpendicular dipole direction, as, for example, from a nonzero angle between the HMM and the minifilament axis. Thus, the fast relaxation process of the positive birefringence would reflect the spinning rotation about the long axis of the minifilament while the slow relaxation process for the negative birefringence component would derive from the tumbling rotation of the long axis.

The semilogarithmic plots of the decay of the slow, negative birefringence component after the electric field is removed of native myosin II and the wild-type and point mutant rod minifilaments at 2 mM Mg^{2+} and of the deletion mutant rod minifilaments at 1 mM Mg^{2+} (shown in the insets in Figure 4) were all well described by single exponentials consistent with well-defined minifilament lengths. The relaxation times, derived from the slopes of these plots, of the wild type and both mutant rod minifilaments (∼100 μs) were significantly shorter than the relaxation time of native myosin II minifilaments (∼220 μs).

The Mg^{2+} dependence of the total birefringence signal (i.e., the sum of the positive and negative signals at the end of the electric field pulse) normalized for field strength and micromolar concentration of protein and measured at an approximately constant pulse length-to-slow component relaxation time ratio was remarkably similar for wild-type rod and native, dephosphorylated myosin II minifilaments (Figure 5). The abrupt change in signal amplitude with Mg^{2+} concentration and the disappearance of the signal at high Mg^{2+} concentration for both indicate a strongly cooperative flexible-to-stiff transition and consequent decrease in the induced dipole moment (*37*). As discussed previously (*23*, *24*), both the long decay time and the ratio of the amplitudes of the fast and slow components of the birefringence signal for native myosin II minifilaments were independent of Mg^{2+} concentration above 1 mM Mg^{2+} but at lower Mg^{2+} concentrations the qualitative nature of the birefringence

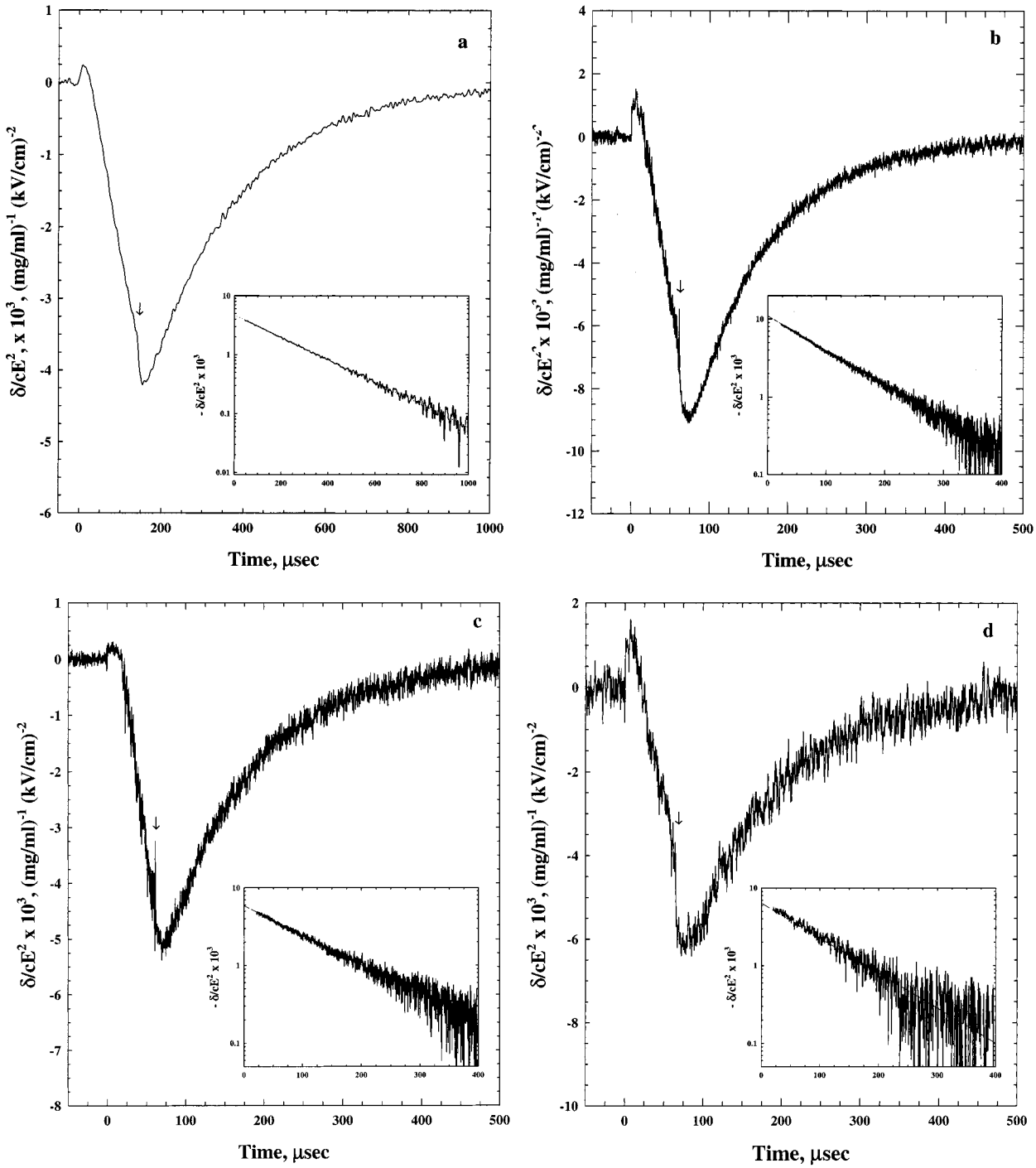

FIGURE 4: Electric birefringence signals and slow component decay kinetics for minifilaments of native *Acanthamoeba* myosin II (a) and wild-type (b), point mutant (c), and deletion mutant (d) rods. The total signal is given as the rotation angle δ (in radians) of the incident plane polarized light, normalized by the protein concentration and applied field strength. The start of the electric field pulse is at $t = 0$; the end is indicated by the arrow. Native myosin II minifilaments (a) were in 2 mM $MgCl_2$, with 1 mM KCl, 1 mM DTT, 2 mM imidazole (pH 7.4), and 5% sucrose, at 20 °C. The protein concentration was 40−50 μg/mL. The signal shown is the average of 25 samples with 32 field pulses each (800 total pulses). The wild-type (b) and point mutant (c) rod samples were also in 2 mM $MgCl_2$, with 2 mM KCl, 1 mM DTT, and 2 mM imidazole (pH 7.4), at 20 °C. The deletion mutant (d) rod minifilaments were in only 1 mM $MgCl_2$, with 2 mM KCl, 1 mM DTT, and 2 mM imidazole (pH 7.4), at 20 °C. Rod protein concentrations were about 20−25 μg/mL, and the signals shown are the average of 6 samples with 32 pulses each (192 total pulses) for the wild-type rods and of 4 samples with 32 pulses each (128 total pulses) for the point and deletion mutant rods. The semilog plots of the normalized birefringence decay after the electric field pulse is removed (time $t =$ 0 now corresponds to the end of the electric field pulse) are shown as figure insets. Only data for the slow component decay are shown (the fast component decay is completed by ~50 μs after the end of the pulse for native myosin II and by ~20 μs for the rods). The dashed lines are the best fits to the data. The good fits for over 95% of the decay indicate that the minifilaments are structurally well-defined and essentially monodisperse. Minifilament lengths can be estimated from the relaxation times. For further details, see Experimental Procedures and Results.

signal changed dramatically, indicating that structures other than octameric minifilaments contributed significantly to the signal. In contrast, the observed signals for the wild-type rod minifilaments were insensitive to Mg^{2+} concentration

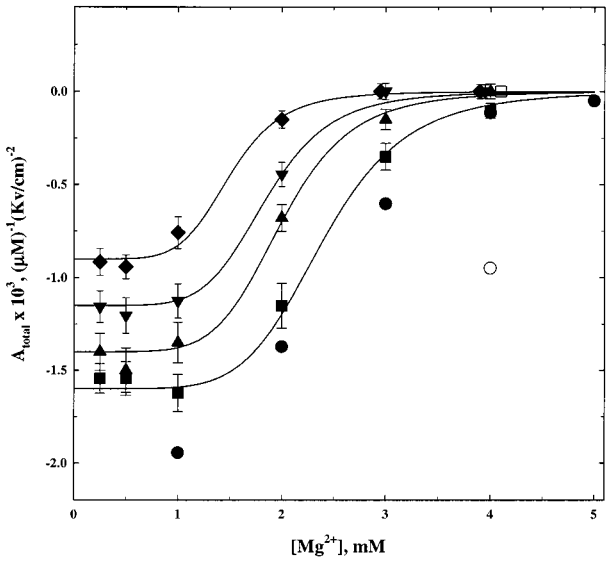

FIGURE 5: [Mg^{2+}] dependence of the birefringence signal intensity of native, dephosphorylated *Acanthamoeba* myosin II (●), wild-type (■), point mutant (▲), deletion mutant (◆), and 1:1 copolymers of wild-type and deletion mutant (▼) rod minifilaments. Signal amplitudes at 4 mM Mg^{2+} with 50 μM ATP added are shown for native dephosphorylated myosin II (○) and for wild-type rod (□). The error bars show the standard deviation from the average of 4−6 measurements. All samples were in 2 mM imidazole (pH 7.4) at 20 °C; the native myosin II samples also contained 1 mM KCl, 1 mM DTT, and 5% sucrose, and the rod samples contained 2 mM KCl, 1 mM DTT, and no sucrose. The dependence of signal amplitude on Mg^{2+} concentration for wild-type rods was insensitive to KCl concentrations between 1 and 5 mM (data not shown). The signal amplitude is the sum of the positive and negative birefringence components at the end of the pulse normalized by protein concentration and applied field strength. The pulse length, ΔT, was 140 μs for myosin II and 65 μs for the rod samples. The ratio of pulse lengths and slow relaxation times, $\Delta T/\tau_{slow}$, was ~0.60−0.65 for all samples, and, therefore, signal amplitudes can be quantitatively compared. Data for rod samples at 0 Mg^{2+} and for native myosin II below 1 mM Mg^{2+} are not shown since minifilaments are not fully assembled, as determined from the slow component relaxation times. Protein concentrations are expressed as micromolar monomer, taking a monomer molecular weight of 410K for native myosin II and 150K for the rods. The solid lines shows the best fits to the rod data assuming that the flexible-to-stiff minifilament transition is coupled to the cooperative binding of six Mg^{2+} ions. The specific equation is: $A_{total} = A_0\{1/[1 + ([Mg^{2+}]/[Mg^{2+}]_{1/2})^6]\}$, where A_0 is the limiting low Mg^{2+} amplitude and $[Mg^{2+}]_{1/2}$ is the Mg^{2+} concentration at the transition midpoint. The best fitting parameters for A_0 and $[Mg^{2+}]_{1/2}$, respectively, are -1.6×10^{-3} and 2.4 mM for the wild-type rod, -1.4×10^{-3} and 2.0 mM for the point mutant, -0.9×10^{-3} and 1.4 mM for the deletion mutant, and -1.15×10^{-3} and 1.85 mM for the wild-type/deletion mutant copolymer. Fits with 4 or 8 cooperatively bound Mg^{2+} are nearly as good.

down to 0.25 mM (Figure 5), indicating that stable minifilaments were formed even at this low Mg^{2+} concentration. The birefringence signals, however, did indicate the existence of a mixture of structures in the absence of Mg^{2+} (data not shown). Given well-defined plateau values of the signal amplitude for wild-type rod minifilaments at high and low Mg^{2+} concentrations, the change in the number (n) of bound Mg^{2+} coupled to the transition can be estimated assuming that the Mg^{2+} ions bind in a single-step reaction. The solid line fit to the wild-type rod data shown in Figure 5 is for $n = 6$. Fits with $n = 4$ or 8 also can adequately describe the data. Unlike native, dephosphorylated myosin II, the birefringence signal amplitude of the wild-type rod minifilaments at high Mg^{2+} concentrations was not affected by the presence of ATP (Figure 5, open symbols). This further supports our previously reported conclusion that the affect of ATP on the flexibility of native, dephosphorylated myosin II (*24*) results from binding of ATP to the N-terminal globular head domain of native myosin II.

Table 3: Electric Birefringence Parameters of Wild-Type and Mutant Rods at 1 mM Mg^{2+} [a]

rod	$-A_{slow}/cE^2$ [(mg/mL)$^{-1}$ (kV/cm)$^{-2}$]	$-A_{fast}/A_{slow}$	τ_{slow} (μs)	$\langle\tau_{fast}\rangle$ (μs)
wild type	0.015 ± 0.002	0.30 ± 0.05	100 ± 10	5 ± 2
point	0.010 ± 0.002	0.10 ± 0.05	105 ± 10	2 ± 1
deletion	0.006 ± 0.001	0.30 ± 0.10	95 ± 15	5 ± 2

[a] The amplitude (in radians) of the slow, negative birefringence component after a 65-μs length electric field pulse, A_{slow}, is corrected for the protein concentration, c, and applied field strength, E. The ratios of the amplitudes of fast and slow birefringence components, A_{fast}/A_{slow}, and their respective relaxation times, $\langle\tau_{fast}\rangle$ and τ_{slow}, were independent of the Mg^{2+} concentration within the low Mg^{2+} plateau regions. At high Mg^{2+} concentrations, the signal was too small to accurately determine these parameters. The fast component relaxation times were determined both from double exponential fits of birefringence curves such as those shown in Figure 4 and from curves obtained with much shorter pulse lengths (~10 μs), but much higher field strengths (~3 kV/cm vs ~ 0.4 kV/cm). Under these conditions, the fast positive birefringence component dominated the overall signal. The fast relaxation times determined by these two methods agreed to within about 20%.

The flexible-to-stiff transition for point mutant rod minifilaments occurred at a slightly lower Mg^{2+} concentration than for wild-type rods and native, dephosphorylated myosin II (Figure 5). The transition occurred at an even lower Mg^{2+} concentration for deletion mutant rods (Figure 5), consistent with the hinge region being the primary source of the Mg^{2+}-dependent flexible-to-stiff transition. The plateau value of the signal amplitude at low Mg^{2+} concentrations (~1 mM and less) for the deletion mutant rod minifilaments was less than that for the point mutant and wild-type rod minifilaments, suggesting these minifilaments were somewhat less flexible than the other two preparations under these conditions. The cooperativity of the transition for the point and deletion mutant rod minifilaments was similar to that seen for the wild type, as shown by the solid line fits to the data with $n = 6$.

The Mg^{2+}-dependent signal amplitudes for minifilament copolymers of 1:1 mixtures of the wild-type and deletion mutant rods are also shown in Figure 5. The signal amplitude at low Mg^{2+} concentrations for the copolymeric minifilaments was intermediate between the wild-type and deletion mutant rod values. The flexible to stiff transition for the copolymeric minifilaments also occurred at an intermediate Mg^{2+} concentration. The cooperativity of the transition, however, was qualitatively similar to that of the pure wild-type or deletion mutant rods. In particular, the transition was not a much broader, two-step change in flexibility that would have been expected for a transition of independent rod monomers. Thus, the transition occurred at the level of the whole minifilament, analogous to observations on native myosin II that functional regulation occurs at the level of the whole minifilament (*15*−*17*).

Table 3 summarizes a number of optical and kinetic parameters extracted from the birefringence experiments at 1 mM Mg^{2+} (the low Mg^{2+} plateau region) for the wild-

type, point mutant, and deletion mutant rod minifilaments.

DISCUSSION

Previous studies had led us to propose (*24*) that an oscillation between stiff and flexible conformations not only accompanied but also was required for the mechanochemical activity of *Acanthamoeba* myosin II minifilaments, and that this requirement could provide the basis for regulation of activity by phosphorylation of the three serine residues in the C-terminal tailpiece. Electric birefringence is a convenient tool for monitoring these changes in flexibility since the induced dipole moment that is responsible for the unusual optical signal of minifilaments is a direct consequence of internal motions of minifilaments. As measured by electric birefringence, minifilaments of enzymatically active, dephosphorylated myosin II dramatically stiffen as the Mg^{2+} concentration is increased into the range needed for optimal actin-activated Mg-ATPase activity (*23*). This stiffening is reversed by ATP or ADP binding (*24*). Minifilaments would, thus, cycle between comparatively stiff and flexible conformations during the ATPase cycle. On the other hand, minifilaments of inactive, phosphorylated myosin II remain flexible at all Mg^{2+} concentrations and are unaffected by bound nucleotide (*24*), and, therefore, cannot undergo the flexible-to-stiff cycle which, we proposed, is required for expression of actin-activated Mg^{2+}-ATPase activity.

The most probable site for the conformational changes responsible for the Mg^{2+}-, phosphorylation-, and ATP-dependent flexible-to-stiff cycle was thought to be the hinge region that defines the HMM−LMM junction and is proximal to the C-terminal phosphorylation sites of other monomers in the minifilament (*22*). This model gains additional support from the data in this paper. The close similarity of the optical signals (Figure 4a,b) and of the change of signal intensities with Mg^{2+} concentration (Figure 5) between native, dephosphorylated myosin II and wild-type rod minifilaments indicates that the Mg^{2+}-dependent flexibility of minifilaments is a property of the rods themselves. Furthermore, the close correspondence of the concentration-normalized total signal amplitudes and the ratios of fast and slow component amplitudes means that the N-terminal globular heads (the S1 domains) contribute almost negligibly to the dipole and birefringence of native myosin minifilaments. This likely reflects the much smaller intrinsic birefringence of S1 heads compared with coiled-coil tails and a cancellation of contributions due to the relative orientation of heads both within a monomer and within the minifilament. A connection between the S1 heads and minifilament flexibility, however, is clearly seen from the effect of nucleotide binding. Although ATP had no effect on the stiffness of rod minifilaments (Figure 5), the flexibility of native, dephosphorylated myosin II minifilaments increases significantly with ATP binding. This supports our previous conclusion (*24*) that the change in the flexibility of native myosin II minifilaments results from the binding of ATP to the N-terminal globular domains.

The major difference between the native myosin II and rod minifilaments is in the relaxation times of the two birefringence components. Analysis of these relaxation times, however, shows that the native myosin II and rod minifilaments are structurally very similar. Previous hydrodynamic modeling of native myosin II minifilaments ($\tau_{slow} = 220\ \mu s$) gave lengths of 210−220 nm, depending on the bend angle at the HMM−LMM junction and on the disposition of the S1 heads (*23*, *24*). Assuming an approximate length of 14 nm for the projection of the S1 heads along the minifilament axis, this corresponds to a length of ∼190 nm between the tips of the rod portions of the terminal HMMs in the antiparallel filament. Similar hydrodynamic calculations for wild-type rod minifilaments ($\tau_{slow} = 100\ \mu s$), assuming an octameric structure and an angle of ∼10−25° between the minifilament long axis and the portion of the rod equivalent to S2 (see below), yield an overall length of ∼185−195 nm. The somewhat larger τ_{slow} for point mutant rods (110 μs) and smaller τ_{slow} for the deletion mutant (95 μs) correspond to length differences of less than 5 nm. The slow component relaxation times of rod minifilaments are consistent with removing the S1 heads from *Acanthamoeba* native myosin II minifilaments.

The bend angle between the S2 equivalent of the wild type rod and the minifilament long axis can be estimated both from the ratio of positive and negative birefringence components and from the fast component relaxation time. From the equations developed previously (*37*), the observed $A_{fast}/A_{slow} = -0.30$ (Table 3) corresponds to an apparent angle of 20−25°, which is comparable to the previous estimate of ∼20° for native myosin II minifilaments (*23*, *24*). However, from hydrodynamic calculations of $\langle\tau_{fast}\rangle$, modeling the minifilament as a set of beads, the estimated angle is only 10−15°. We do not know if the discrepancy in the bend angle of the wild-type rods calculated by the two methods is due to shortcomings in the hydrodynamic calculations of the fast spinning rotations or in the theory used to describe the optical signal. The $\langle\tau_{fast}\rangle$ for minifilaments of native myosin II depends too strongly on the orientation of the S1 heads to be useful for calculating the bend angle of native myosin II minifilaments. In any case, it is clear that the basic minifilament structures of native *Acanthamoeba* myosin II and wild-type rods are very similar. The large difference in the relaxation times of their negative birefringence signals reflects simply the presence or absence of the S1 heads which contribute substantially to the hydrodynamics but minimally to the dipole moment and birefringence amplitude of myosin II minifilaments.

The birefringence data are also informative about the effects of the point and deletion mutations at or around proline-1244 on the properties of the hinge. Compared with wild-type minifilaments, τ_{slow} for the point mutant rod minifilaments was only slightly larger, but both τ_{fast} and $-A_{fast}/A_{slow}$ were substantially smaller (Table 3). The latter two parameters are indicative of a smaller bend angle for the HMM−LMM hinge: ∼15°, calculated from $-A_{fast}/A_{slow}$; and ∼8°, calculated from τ_{fast}, compared to 20−25° and 10−15°, respectively, for wild-type rod minifilaments. This suggests that proline-1244 might be a prime determinant of this angle. The deletion mutant data, however, indicate that this interpretation may be too simple. The observed τ_{slow} for deletion mutant rod minifilaments, was only slightly smaller than for the wild-type minifilaments, and, surprisingly, both $-A_{fast}/A_{slow}$ and τ_{fast} were very similar to the values for wild-type rod minifilaments, and significantly different than the values for the point mutant rod minifilaments (Table 3).

These data indicate that the apparent bend angles between the HMM and LMM domains are very similar for the deletion mutant and wild-type rod. We do not understand why the point and deletion mutant rod minifilaments have different apparent bend angles. We would point out, however, that the 25 amino acids removed from the deletion mutant rods correspond to about 90° of helical turn in a coiled-coil that may affect interactions between the HMM and other regions of the minifilament.

A principal difference between the wild-type and mutant rod minifilaments was the Mg^{2+} dependence of the flexible-to-stiff transitions (Figure 5). Although the signal amplitudes in the low Mg^{2+} plateau region were very similar for wild-type and point mutant rod minifilaments, the cooperative transition from flexible-to-stiff conformations occurred at a somewhat lower Mg^{2+} concentration for the point mutant rods. The deletion mutant rod minifilaments had a lower signal amplitude in the low Mg^{2+} region than either the point mutant or the wild-type rod minifilaments, and the transition between flexible and stiff conformations occurred at an even lower Mg^{2+} concentration. The stiff conformation is most stable for deletion mutant minifilaments, followed by point mutant, then, finally, wild-type rod minifilaments. This ordering is qualitatively consistent with the predictions of the programs Paircoil and Coils for the stability of the α-helical coiled-coil in the hinge region, suggesting that the flexible-to-stiff transition might reflect a localized melting or weakening transition of the α-helical coiled-coil at the HMM−LMM junction. Since the apparent cooperativity of the transition is very similar for the three rod minifilaments (within experimental error), an extra energy stabilizing the stiff conformation can be estimated from the ratio of Mg^{2+} concentrations at the transition midpoint and the number of extra Mg^{2+} ions that bind, if the Mg^{2+} binding sites are unchanged. Assuming $\sim 6 \pm 2$ extra bound Mg^{2+}/minifilament (see Results), the shift in the transition midpoint corresponds to a stabilizing energy difference of 2 ± 1 kcal/mol between wild-type rod and point mutant rod minifilaments and 6 ± 3 kcal/mol between wild-type rod and deletion mutant rod minifilaments. These comparatively small increases in the apparent stability of the stiff conformation are qualitatively consistent with the small increase in unfolding temperature of the deletion mutant rod monomer (only ∼1−2 °C) compared with the native rod in 0.6 M KCl without added Mg^{2+} (*25*).

What might be the structural basis of the Mg^{2+} dependence of the flexible-to-stiff transition at the HMM−LMM junction? The differences in electric birefringence between the mutant and wild-type rod minifilaments are not as dramatic as predicted by Paircoil and Coils. Although a 100% probability of coiled-coil is predicted for the deletion mutant rods, these minifilaments are flexible at low Mg^{2+} concentrations. Therefore, there seem likely to be important determinants of stability near the HMM−LMM junction that are not accounted for by either Paircoil or Coils. The apparent coupling of Mg^{2+} binding and minifilament flexibility suggests that the balance of negative and positive charges in this region may be important. Sequences on both sides of the hinge region (residues 1230−1254) are highly negatively charged. Between residues 1204 and 1218, there are 4 aspartates, 2 glutamates, and only 1 neutralizing arginine, and between residues 1258 and 1273, there are 7 glutamates and 1 arginine (Figure 1). In the minifilament, the apposition of C-terminal tailpieces and hinge regions of adjacent rods could bring an additional five arginine and two glutamates per heavy chain into this region (Figure 1). This envelope of negative charges around a sequence with inherent, impaired probability to form a coiled-coil may be the basis of the Mg^{2+}-dependent flexible-to-stiff conformational change of rod and myosin II minifilaments and the associated change in actin-activated Mg-ATPase activity of minifilaments of dephosphorylated myosin II. Conversely, the addition of up to six more negative charges per heavy chain by enzymatic phosphorylation of three serine residues in the C-terminal tailpiece of native myosin II may lock the minifilaments into a flexible, enzymatically inactive conformation reversible only by dephosphorylation.

ACKNOWLEDGMENT

We thank Dr. James Sellers for advice on performing the PAIRCOIL analysis, Dr. Brian Martin for N-terminal microsequencing of rod preparations, and Mrs. Angela Corigliano-Murphy for measuring the rod concentrations by amino acids analysis.

REFERENCES

1. Maruta, H., and Korn, E. D. (1977) *J. Biol. Chem. 252*, 6501−6509.
2. Pollard, T. D., Stafford, W. F., III, and Porter, M. E. (1978) *J. Biol. Chem. 253*, 4798−4808.
3. Atkinson, M. A. L., and Korn, E. D. (1986) *J. Biol. Chem. 261*, 3382−3388.
4. Atkinson, M. A. L., Robinson, E. A., Appella, E., and Korn, E. D. (1986) *J. Biol. Chem. 261*, 1844−1848.
5. Hammer, J. A., III, Bowers, B., Paterson, B. M., and Korn, E. D. (1987) *J. Cell Biol. 105*, 913−925.
6. Sinard, J. H., Stafford, W. F., III, and Pollard, T. D. (1989) *J. Cell Biol. 109*, 1537−1547.
7. Sinard, J. H., Rimm, D. L., and Pollard, T. D. (1990) *J. Cell Biol. 111*, 2417−2426.
8. Cote, G. P., Collins, J. H., and Korn, E. D. (1981) *J. Biol. Chem. 256*, 12811−12816.
9. Collins, J. H., Cote, G. P., and Korn, E. D. (1982) *J. Biol. Chem. 257*, 4529−4534.
10. Cote, G. P., Robinson, E. A., Appella, E., and Korn, E. D. (1984) *J. Biol. Chem. 259*, 12781−12787.
11. Kuznicki, J., Cote, G. P., Bowers, B., and Korn, E. D. (1985) *J. Biol. Chem. 260*, 1967−1972.
12. Ganguly, C., Baines, I. C., Korn, E. D., and Sellers, J. (1992) *J. Biol. Chem. 267*, 20900−20904.
13. Brzeska, H., and Korn, E. D. (1996) *J. Biol. Chem. 271*, 16983−16986.
14. Sellers, J. R., and Goodson, H. V. (1995) in *Protein Profile* (Sheterlin, P., Ed.) Vol. 2, pp 1323−1423, Academic Press Ltd., London.
15. Kuznicki, J., Albanesi, J. P., Cote, G. P., and Korn, E. D. (1983) *J. Biol. Chem. 258*, 6011−6014.
16. Atkinson, M. A. L., Lambooy, P. K., and Korn, E. D. (1989) *J. Biol. Chem. 264*, 4127−4132.
17. Ganguly, C., Atkinson, M. A. L., Sathymoorthy, V., Bowers, B., and Korn, E. D. (1990) *J. Biol. Chem. 265*, 9993−9998.
18. Redowicz, M. J., Martin, B., Zolkiewski, M., Ginsburg, A., and Korn, E. D. (1994) *J. Biol. Chem. 269*, 13558−13563.
19. Zolkiewski, M., Redowicz, M. J., Korn, E. D., and Ginsburg, A. (1995) *Arch. Biochem. Biophys. 318*, 207−214.
20. Lupas, A. (1996) *Trends Biochem. Sci. 21*, 375−382.
21. Wijmenga, S. S., Atkinson, M. A. L., Rau, D. C., and Korn, E. D. (1987) *J. Biol. Chem. 262*, 15803−15808.
22. Atkinson, M. A. L., and Korn, E. D. (1987) *J. Biol. Chem. 262*, 15809−15811.

23. Rau, D. C., Ganguly, C., and Korn, E. D. (1993) *J. Biol. Chem. 268*, 4612−4621.
24. Redowicz, M. J., Korn, E. D., and Rau, D. C. (1996) *J. Biol. Chem. 271*, 12401−12407.
25. Zolkiewski, M., Redowicz, M. J., Korn, E. D., Hammer, J. A., III, and Ginsburg, A. (1997) *Biochemistry 36*, 7876−7883.
26. Collins, J. H., and Korn, E. D. (1980) *J. Biol. Chem. 255*, 8011−8014.
27. Collins, J. H., and Korn, E. D. (1981) *J. Biol. Chem. 256*, 2586−2595.
28. Tyler, J. M., and Branton, D. (1980) *J. Ultrastruct. Res. 71*, 95−102.
29. Shapiro, B. M., and Ginsburg, A. (1968) *Biochemistry 7*, 2153−2167.
30. McMeekin, T. L., and Marshall, K. (1952) *Science 116*, 142−143.
31. Stafford, W. F., III (1992) *Anal. Biochem. 203*, 295−301.
32. Stafford, W. F., III (1996) *Biophys. J. 70*, A231.
33. Stafford, W. F., III (1997) *Curr. Opin. Biotechnol. 8*, 14−24.
34. Garcia de la Torre, J., and Bloomfield, V. A. (1981) *Q. Rev. Biophys. 14*, 81−139.
35. Fraser, R. D. B., and MacRae, T. P. (1973) *Conformation in Fibrous Proteins*, Academic Press, Inc., New York.
36. McLachlan, A. D. (1984) *Annu. Rev. Biophys. Bioeng. 13*, 167−189.
37. Rau, D. C. (1993) *J. Biol. Chem. 268*, 4622−4624.
38. Berger, B., Wilson, D. B., Wolf, E., Tonchev, T., Milla, M., and Kim, P. S. (1995) *Proc. Natl. Acad. Sci. U.S.A. 92*, 8259−8263.
39. Lupas, A. (1996) *Methods Enzymol. 260*, 513−525.
40. Schachman, H. K. (1959) *Ultracentrifugation in Biochemistry*, Academic Press, New York.
41. Pollard, T. D. (1982) *J. Cell Biol. 95*, 816−825.

BI982679D